Hindawi
Journal of Chemistry
Volume 2019, Article ID 5638590, 10 pages
https://doi.org/10.1155/2019/5638590

Research Article

Structure and Electrochemical Behavior of Minor Mn-Doped Olivine $LiMn_xFe_{1-x}PO_4$

Le Thanh Nguyen Huynh,[1,2] **Pham Phuong Nam Le**,[1] **Viet Dung Trinh**,[3] **Hong Huy Tran**,[1] **Van Man Tran**,[1,2] **and My Loan Phung Le**[1,2]

[1]*Applied Physical Chemistry Laboratory (APCLAB), VNUHCM-University of Science, Ho Chi Minh City, Vietnam*
[2]*Department of Physical Chemistry, Faculty of Chemistry, VNUHCM–University of Science, Ho Chi Minh City, Vietnam*
[3]*School of Chemical Engineering, Hanoi University of Science and Technology, Hanoi, Vietnam*

Correspondence should be addressed to Le Thanh Nguyen Huynh; hltnguyen@hcmus.edu.vn

Received 8 September 2019; Revised 20 October 2019; Accepted 24 October 2019; Published 26 December 2019

Guest Editor: Chu Liang

In the recent years, olivine $LiFePO_4$ has been considered as a prospective cathode material for lithium-ion batteries. However, low conductivity is an obstacle to the commercialization of $LiFePO_4$; doping the transition metal such as Mn and Ni is one of the solutions for this issue. This work aimed to synthesize the Mn-doped olivines $LiMn_xFe_{1-x}PO_4$ at low content of Mn ($x = 0.1, 0.2$) via the hydrothermal route followed by pyrolyzed carbon coating. The synthesized olivines were well crystallized in olivine structure, with larger lattice parameters compared with $LiFePO_4$. The EXD and TGA results confirmed the coated carbon of 4.14% for $LiMn_{0.1}Fe_{0.9}PO_4$ and 6.86% for $LiMn_{0.2}Fe_{0.8}PO_4$. Both of Mn-doped olivines showed higher diffusion coefficients of Li^+ intercalation than those of $LiFePO_4$ that led a good performance in the cycling test. $LiMn_{0.2}Fe_{0.8}PO_4$ exhibited a higher specific capacity (160 mAh/g) than $LiMn_{0.1}Fe_{0.9}PO_4$ (155 mAh/g), and the Mn content is beneficial for the cycling performance as well as ionic conductivity.

1. Introduction

In the last three decades, the world has witnessed urges for significant breakthroughs in the hi-tech industry. Among them, the demand for power storage can provide a large amount of energy with good cycling performance. Lithium-ion batteries (LIBs) have taken those requirements as their advantages. A great deal of research studies have delved deeply into the topic of LIBs in order to develop suitable materials to improve the performance of batteries. The use of cathode materials for LIBs has been an attractive field because they are the determining factor of power density, capacity, lifetime, and cost of the batteries [1, 2]. Besides the popular layered transition metal oxides, olivine materials $LiMPO_4$ (M = Mn, Co, Fe, ...), represented by $LiFePO_4$, are competitive candidates to the commercialized $LiCoO_2$. They are of low cost and easy to synthesize and nontoxic. High thermal stability and comparable specific capacity (170 mAh/g) to $LiCoO_2$ (140 mAh/g) are the key to their large-scale application in the future [3, 4].

Olivine materials are categorized as orthorhombic structures with the space group Pnma. The lattice of $LiFePO_4$ contains [FeO_6] octahedral sites and [PO_4] tetrahedral sites sharing vertices and edges. The octahedrons are connected to form a tunnel structure, which facilitates the migration of Li^+ ions [5]. The alternate arrangement of [FeO_6] and [PO_4] groups, however, leads to low conductivity (~10^{-9} S/cm at room temperature), which is the main limitation of $LiFePO_4$ [6]. In order to solve this issue, many research projects have focused on minimizing the particle size to nanoscale with a modern synthetic process. Besides, doping the material with Mn or Ni ($LiMn_xFe_{1-x}PO_4$ or $LiNi_xFe_{1-x}PO_4$) is also a promising solution [7]. Nakamura et al. reported that the Mn^{2+} substitution in olivine compounds (prepared by the solid-state reaction) expended the unit cell along the *c*-axis, which facilitated the Li immigration in doped olivines, and

Li^+ diffusions were found to be in the order of 10^{-12} cm^2/s [8]. Novikova et al. prepared the olivines $LiMn_xFe_{1-x}PO_4$ ($x = 0$–0.4) by the sol-gel method, and the particles varied in the range of 400 nm to 4 μm. By using Mössbauer spectroscopy, they proved the low-content Mn doping ($x = 0.1$, 0.2) enhanced the discharge capacity to 142 mAh/g (at the current density of 55 mA/g) due to the solid solution formation under gradual changes in the potential of Mn [9].

Our work aimed to synthesize the Mn-doped olivine $LiMn_xFe_{1-x}PO_4$ at low-content of Mn doping ($x = 0.1$, 0.2) via the hydrothermal route followed by pyrolyzed carbon coating. The structure and morphology of the synthesized olivines were evaluated by X-ray diffraction and FE-SEM coupling with EDX and TGA. We also considered the kinetics of Li^+ intercalation (lithium diffusion coefficient, D_{Li}) determined from cyclic voltammetry results, which are related to the cycling performance.

2. Methods

2.1. Preparation of $LiMn_xFe_{1-x}PO_4$. Mn-doped olivines $LiMn_{0.1}Fe_{0.2}PO_4$ and $LiMn_{0.2}Fe_{0.8}PO_4$ were synthesized via the hydrothermal method. 150 mL of aqueous solution of $Mn(CH_3COO)_2.4H_2O$ and $Fe(NO_3)_3.9H_2O$ (at the molar ratio of 1 : 9 or 2 : 8) with a small amount of n,n-dimethylformamide C_3H_7NO as the reducing agent was stirred at 80°C for 1 hour. The solution was then mixed with $LiOH.H_2O$, H_3PO_4, $C_6H_8O_6$, and HNO_3 and stirred thoroughly at ambient condition for 6 hours using a magnetic stirrer. The mixture was transferred into a hydrothermal system and annealed at 180°C for 12 hours. The outcome was separated from the suspension by the centrifuge and low-pressure filter, then washed by deionized water, and finally dried at 60°C overnight. In order to coat carbon on the surface of the synthesized olivines, the obtained solid was grounded with glucose at the mass ratio of 1 : 1 and then calcined at 700°C in N_2/Ar atmosphere (95/5, v/v) for 3 hours.

2.2. Structural, Morphological, and Electrochemical Characterizations. The crystalline structure of the synthesized olivines was characterized by X-ray diffraction using D8-ADVANCED (Bruker, Cu$K\alpha$ radiation) in the 2θ range of 10–70° at the scanning rate of 0.020°C/step. The morphology and elemental composition were evaluated by scanning electron microscopy (SEM) and SEM-EDX using a Hitachi FE-SEM S-4800 scanning electron microscope. The proportion of carbon coating on the particles was quantified by thermal analysis from 25°C to 800°C in air at the scanning rate of 10°C/min using a LABSYS evo TG–DSC 1600 system (Setaram, France).

The cathode slurry was prepared by mixing 90 wt% active materials, 7.5 wt% graphite, 7.5% acetylene black, and 5 wt% polyvinylidene fluoride-co-hexafluoropropylene (PVDF-HFP) in N-methyl-2-pyrrolidone (NMP). The slurry then was coated on the aluminum foil with a thickness of 50 μm and density of 2 mg/cm^2. The olivine electrodes were cut with a diameter of 10 mm and dried at 130°C under vacuum for 24 hours. The two-electrode Swagelok-type cells were assembled in an Ar-filled glovebox, and the cell consisted of an olivines electrode as the positive electrode, lithium foil as the negative electrode, three glass Whatman microfibers as the seperator, and 100 mL of 1 M $LiPF_6$ in a mixture of ethylene carbonate (EC) and dimethyl carbonate (DMC) at a volumetric ratio of 2 : 1 as the electrolyte.

The electrochemical behaviors of Mn-doped olivines were evaluated by cyclic voltammetry (CV) and galvanostatic cycling test using the apparatus VSP (BioLogic, France). The cyclic voltammetry (CV) was carried out in a potential range of 2.5–4.5 V (versus Li^+/Li) in the various rates from 20 μV/s to 120 μV/s. The cycling tests were conducted at rate C/10.

3. Results and Discussion

3.1. Structure and Morphology. The X-ray diffraction patterns of two Mn-doped olivines (Figures 1(a) and 1(b)) can be indexed in an orthorhombic structure with the space group Pnmb. Results of Rietveld refinement, gathered in Table 1, are in good agreement with the original olivine structure (JSPDF: 01-083-2092). The Li atoms are located at 4a sites; the Fe, Mn, and P atoms are in 4c sites; and the O atoms are in 8a sites. The fractions of Mn : Fe are 0.1 : 0.9 and 0.2 : 0.8, which approximately match the EDX results. The X-ray diffraction patterns indicate the presence of a pure and very well crystallized single phase without the impurity phase (e.g., MnO_2, Li_2O, and Fe_2O_3). It is obvious that partially replacing Fe with Mn amplifies the size of the olivines lattice unit, which can be explained by the fact that the ionic radius of Mn^{2+} (80 pm) is superior to that of Fe^{2+} (78 pm). This result agrees with previous reports about Mn-doped olivine [10–13].

Morphology of two Mn-doped olivines was analyzed by scanning electron microscopy. The hydrothermal preparation led to a homogeneous distribution. It can be seen (Figure 2) that the particle grains of both samples point out the polyhedral shapes at submicrometric scale (approximately 200–400 nm). According to EDX data in Figure 3 and Table 2, the elemental composition of Li, Fe, Mn, and P in the samples corresponds to the stoichiometric relationship which is suitable to the theoretical composition of $LiMn_{0.1}Fe_{0.9}PO_4$ and $LiMn_{0.2}Fe_{0.8}PO_4$.

Figure 4 shows the TEM images of two Mn-doped olivines, and we observed clearly that the particles' size was in the range of 100-200 nm. The TEM images were coherent to SEM images. The Raman spectra of two Mn-doped olivines in Figure 5 show two fingerprint signals of carbon in the high-frequency region at 1385 cm^{-1} (D-band) and 1583 cm^{-1} (G-band) that confirm the composites between Mn-doped olivine and carbon $LiMn_xFe_{1-x}PO_4$@C [14–17].

Thermal gravity analysis (TGA) is useful to quantify the proportion of coated carbon in Mn-doped samples. Figure 6 demonstrates the TGA curves of two Mn-doped olivines acquired in air at 10°C/min in the temperature range of 25–800°C. The increase in mass from 300°C to 400°C is caused by the oxidation of Fe and Mn elements in the samples to form metal oxides. At a temperature higher than

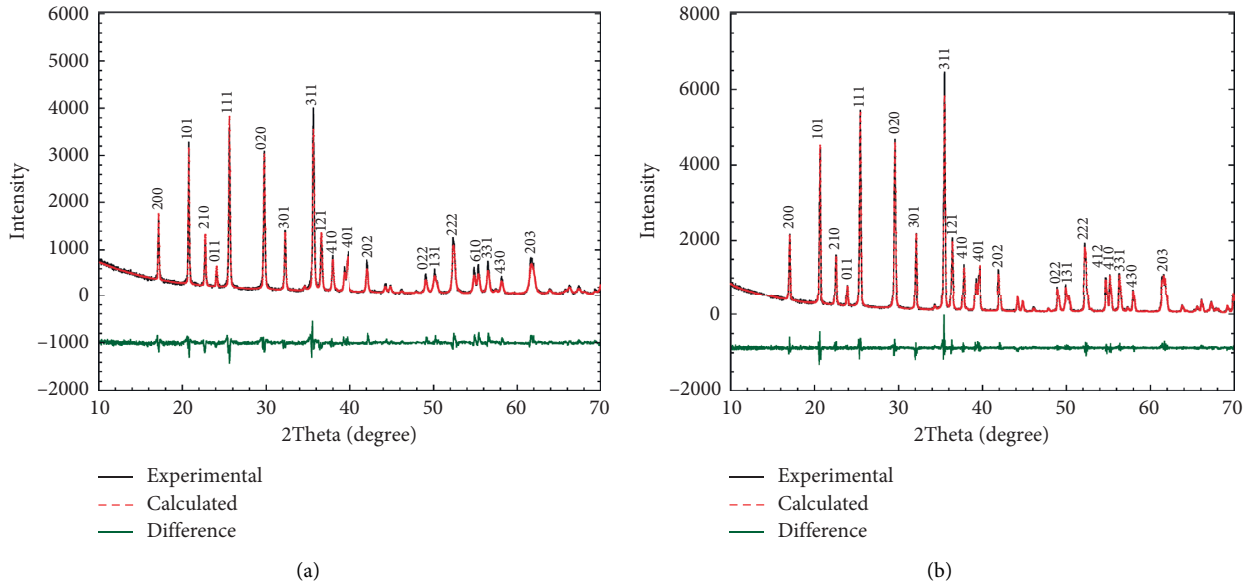

Figure 1: XRD patterns of $LiMn_{0.1}Fe_{0.9}PO_4$ (a) and $LiMn_{0.2}Fe_{0.8}PO_4$ (b).

Table 1: Lattice parameters of $LiMn_{0.1}Fe_{0.9}PO_4$ and $LiMn_{0.2}Fe_{0.8}PO_4$.

	a (Å)	b (Å)	c (Å)	V (Å^3)
$LiMn_{0.1}Fe_{0.9}PO_4$	6.015(4)	10.346(1)	4.7050	292.82
$LiMn_{0.2}Fe_{0.8}PO_4$	6.041(5)	10.384(1)	4.7222	296.24
$LiFePO_4$ [4]	6.008(3)	10.334(4)	4.693(1)	291.39
$LiMnPO_4$ [11]	10.452(1)	6.106(1)	4.746(1)	302.90

400°C, the mass of each sample shows a steady decline that results from the reaction between carbon and oxygen [18]. The amount of carbon in each sample is the difference in mass percentage measured at 400°C and 800°C. Figure 6 infers that the carbon content in $LiMn_{0.1}Fe_{0.9}PO_4$ (6.86%) is higher than that in $LiMn_{0.2}Fe_{0.8}PO_4$ (4.14%).

3.2. Electrochemical Behaviors. The Li insertion into the original olivine phase is described by the domino-cascade mechanism between two phases $LiFePO_4$ and $FePO_4$ with the characteristic voltage at 3.45 V (vs. Li^+/Li), corresponding to the redox couple Fe^{3+}/Fe^{2+}. The Mn doping into olivine can add a signal of redox couple Mn^{3+}/Mn^{2+} around 4 V, and the intensity of signal depends on the Mn content in olivine, in the potential range of 2.5–4.5 V with the scan rate s. Figures 7(a) and 7(b) demonstrate the cyclic voltammograms of $LiMn_{0.1}Fe_{0.9}PO_4$ and $LiMn_{0.2}Fe_{0.8}PO_4$ in various scan rates from 20 to 120 μV/s. The strong and shaped peaks at ~3.5 V in all CV curves are evidenced as the original redox reaction, while the signals at 3.8–4.0 V can be assigned to the doping element reaction. The higher the scanning rate, the higher the peak separation and intensity of $LiMn_{0.2}Fe_{0.8}PO_4$; the Mn signal looks more significant that proposes more capacity contribution in the galvanostatic test.

During the Li intercalation process, Li^+ ions migrated following the 1D channels along the (010) plane in the orthorhombic structure; thus, Li mobility (also called kinetic of intercalation process) affects the electrode performance in the galvanostatic cycling test and habitually determined through the diffusion coefficient (D_{Li}). In our case, kinetics of Li intercalation process into the Mn-doped olivines was assessed by cyclic voltammetry. The scattered plot of cathodic peak current versus square root of scan rates was built up based on CV results and presented in Figure 7(c). Diffusion coefficients of the Li^+ insertion process (D_{Li}) were determined by using the Randles–Sevcik equation:

$$i_p = 2.69 \times 10^5 n^{3/2} A C_{Li} D_{Li}^{1/2} v^{1/2}, \quad (1)$$

where A is the surface area of the cathode (0.785 cm^2); C is the concentration of Li^+ ions in the material (cm^3/mol); and n is the number of transferred electron ($n = 1$). Figure 7(c) shows a linear proportion between i_{pc} and $v^{1/2}$ with the correlation coefficient R^2~1. D_{Li} values calculated from the Randles–Sevcik equation are listed in Table 3. D_{Li} value of $LiMn_{0.2}Fe_{0.8}PO_4$ (9.53×10^{-12} cm^2/s) is four times higher than that of $LiMn_{0.1}Fe_{0.9}PO_4$ (2.81×10^{-12} cm^2/s). According to previous publications, diffusion coefficients of $LiFePO_4$ were obtained between $10^{-14} - 10^{-13}$ cm^2/s [15, 19, 20]. Therefore, partial Mn substitution in the olivine structure benefits the ionic conductivity through the soar of D_{Li}, compared with the original olivine phase.

Cycling performances of two Mn-doped olivines were executed at rate C/10 in the voltage range of 2.5–4.5 V (vs. Li^+/Li). Figure 8 compares the first galvanostatic curve of two doping olivines which demonstrate two Li insertion regions: (i) well-defined plateau at 3.5 V and (ii) the short one at 3.7–4.0 V. We observed the Mn-couple capacity contribution in $LiMn_{0.2}Fe_{0.8}PO_4$ (~30 mAh/g) was higher than its in $LiMn_{0.1}Fe_{0.9}PO_4$ (~10 mAh/g). These results are coherent with the CV′ results. The discharged capacities are found out to be 158 mAh/g for $LiMn_{0.1}Fe_{0.9}PO_4$ and 160 mAh/g for $LiMn_{0.2}Fe_{0.8}PO_4$.

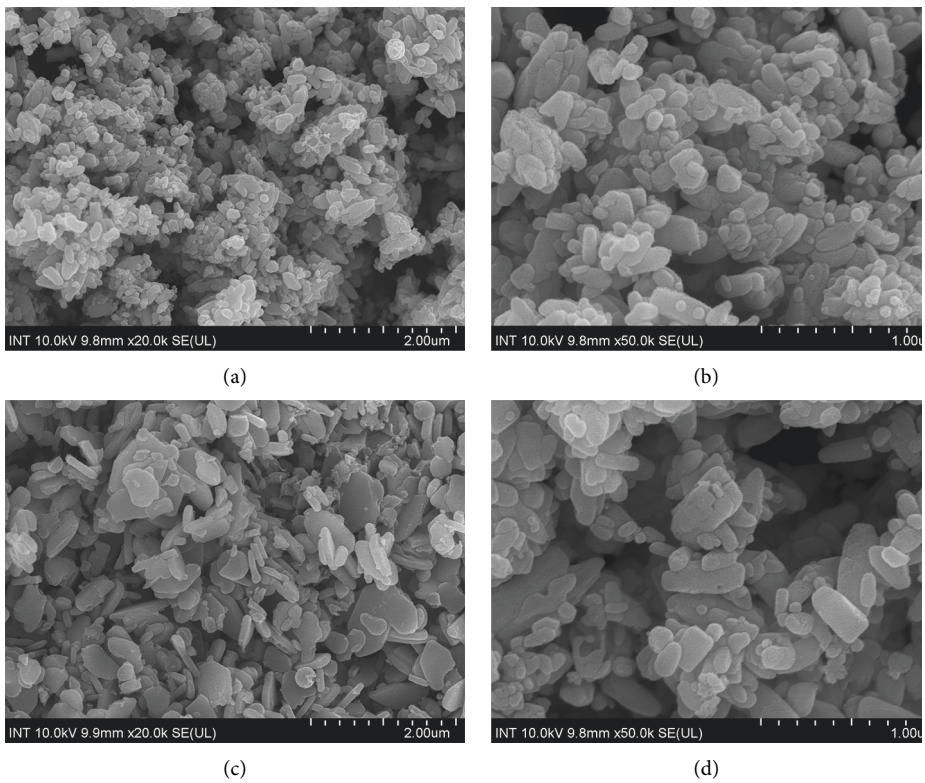

(a) (b)

(c) (d)

Figure 2: SEM images of $LiMn_{0.1}Fe_{0.9}PO_4$ (a, b) and $LiMn_{0.2}Fe_{0.8}PO_4$ (c, d).

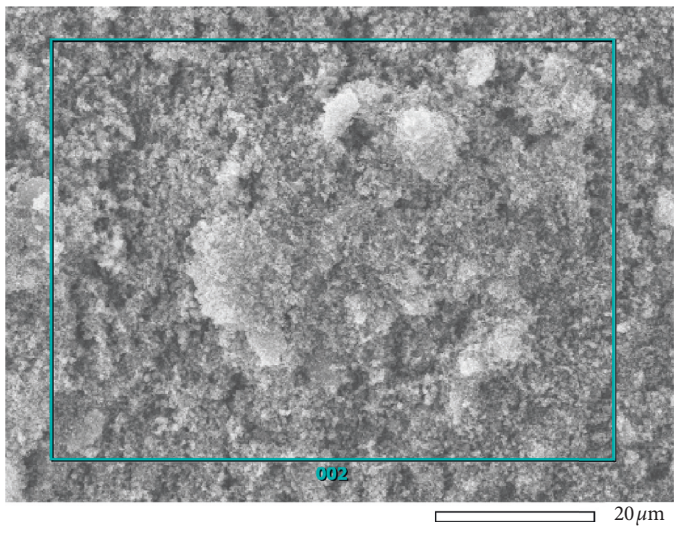

(a)

Figure 3: Continued.

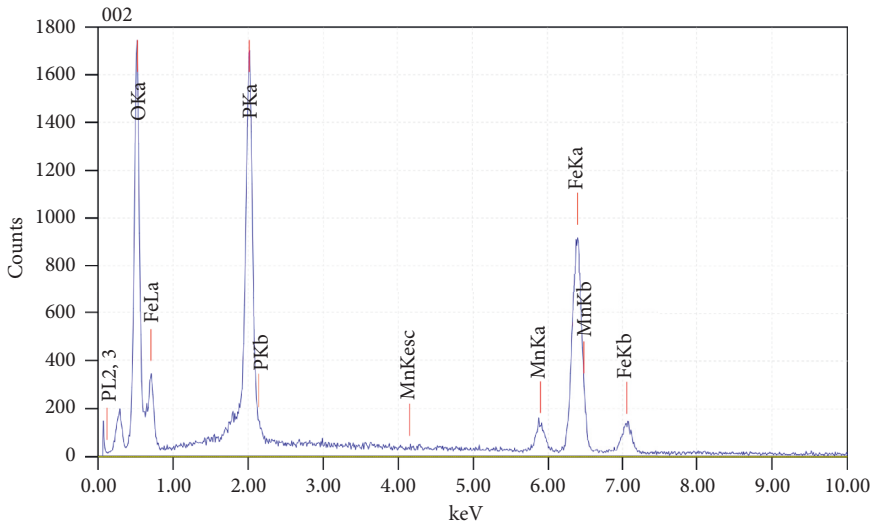

(b)

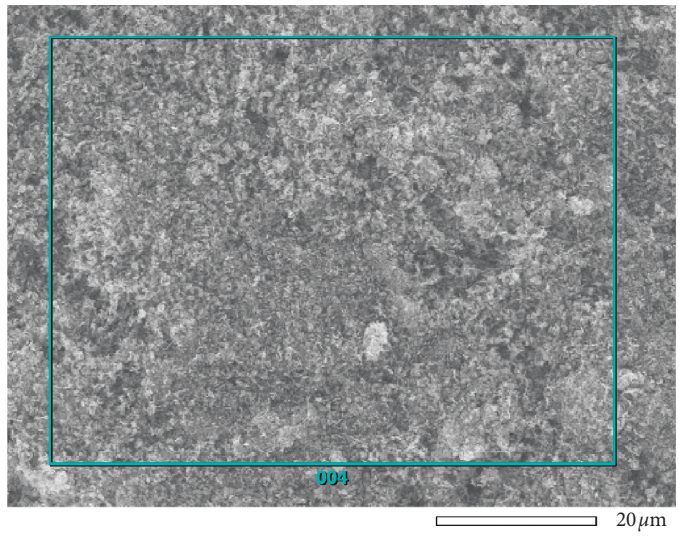

(c)

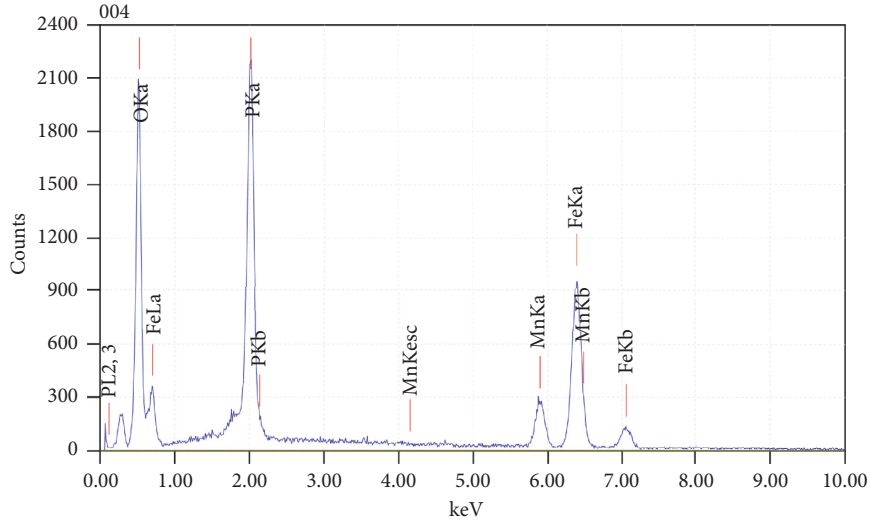

(d)

Figure 3: EDX spectra of $LiMn_{0.1}Fe_{0.9}PO_4$ (a, b) and $LiMn_{0.2}Fe_{0.8}PO_4$ (c, d).

Table 2: Elemental composition of $LiMn_{0.1}Fe_{0.9}PO_4$ and $LiMn_{0.2}Fe_{0.8}PO_4$ determined by SEM-EDX.

	Element	keV	Mass%	Atom%	Ratio Mn : Fe
$LiMn_{0.1}Fe_{0.9}PO_4$	Oxygen	0.525	38.38	63.50	**0.09 : 0.9**
	Phosphorous	2.013	19.08	16.31	
	Manganese	5.894	3.58	1.73	
	Ferrous	6.398	38.95	18.46	
$LiMn_{0.2}Fe_{0.8}PO_4$	Oxygen	0.525	38.74	63.46	**0.18 : 0.8**
	Phosphorous	2.013	20.52	17.36	
	Manganese	5.894	7.44	3.55	
	Ferrous	6.398	33.30	15.63	

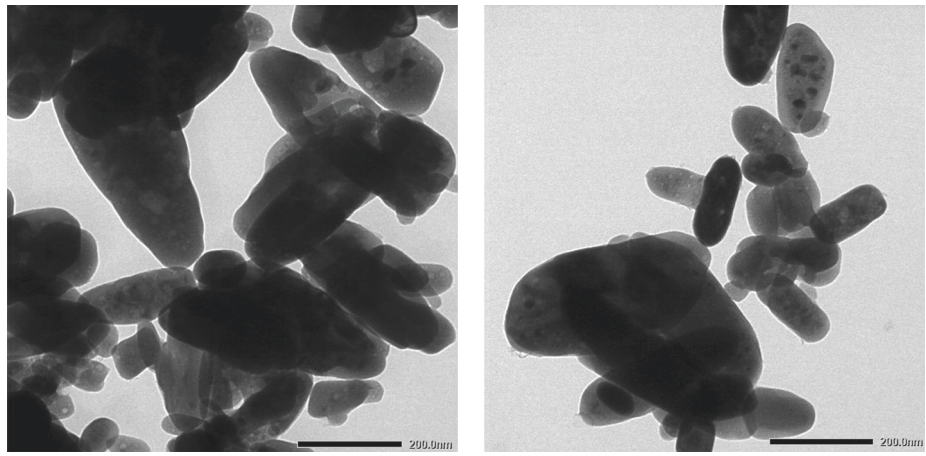

(a) (b)

Figure 4: TEM images of $LiMn_{0.1}Fe_{0.9}PO_4$ (a) and $LiMn_{0.2}Fe_{0.8}PO_4$ (b).

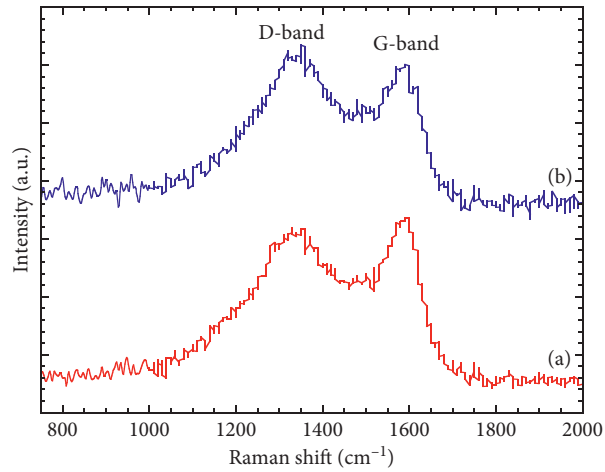

Figure 5: Raman spectra of $LiMn_{0.1}Fe_{0.9}PO_4$ (a) and $LiMn_{0.2}Fe_{0.8}PO_4$ (b).

As shown in Figure 9(a), the discharge curves of $LiMn_{0.1}Fe_{0.9}PO_4$ practically superimpose without any hysteresis, and the capacity is stable at 158 mAh/g upon 50 cycles. In case of $LiMn_{0.2}Fe_{0.8}PO_4$, the Mn capacity contribution is faded cycle by cycle; after 50 cycles, the Mn capacity region at 3.7 V seems to disappear, leading to the decline of discharge capacity to 140 mAh/g. The fading capacity is interpreted by the release of Mn during the charge-discharge process. The Coulombic efficiencies of over 97% (Figure 9(c)) are retained during the cycling test, which indicates a reversible Li intercalation into the olivine hosts.

The rate capability performance of Mn-doped olivines is demonstrated in Figure 9(d), in which current density was set up from C/10 to 5C (1C corresponds to 165 mAh/g). The Mn-doped olivines show a stable capacity, for instance $LiMn_{0.1}Fe_{0.9}PO_4$, 155, 147, 139, 130, 115, and 87 mAh/g at C/

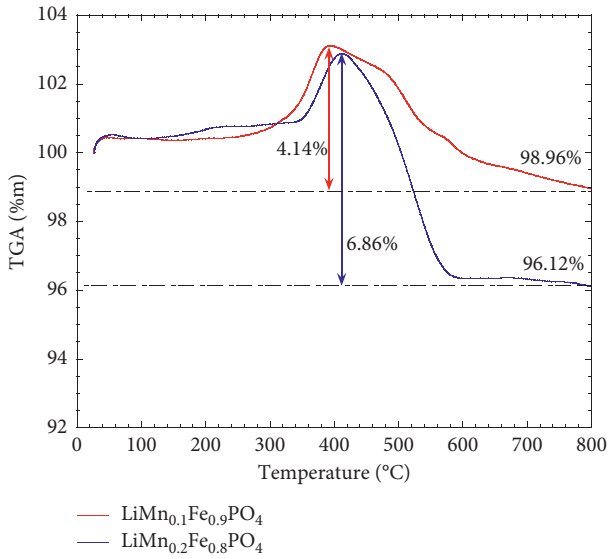

Figure 6: TGA curves of $LiMn_{0.1}Fe_{0.9}PO_4$ and $LiMn_{0.2}Fe_{0.8}PO_4$, acquired in air at 10°C/min in the temperature range of 25–800°C.

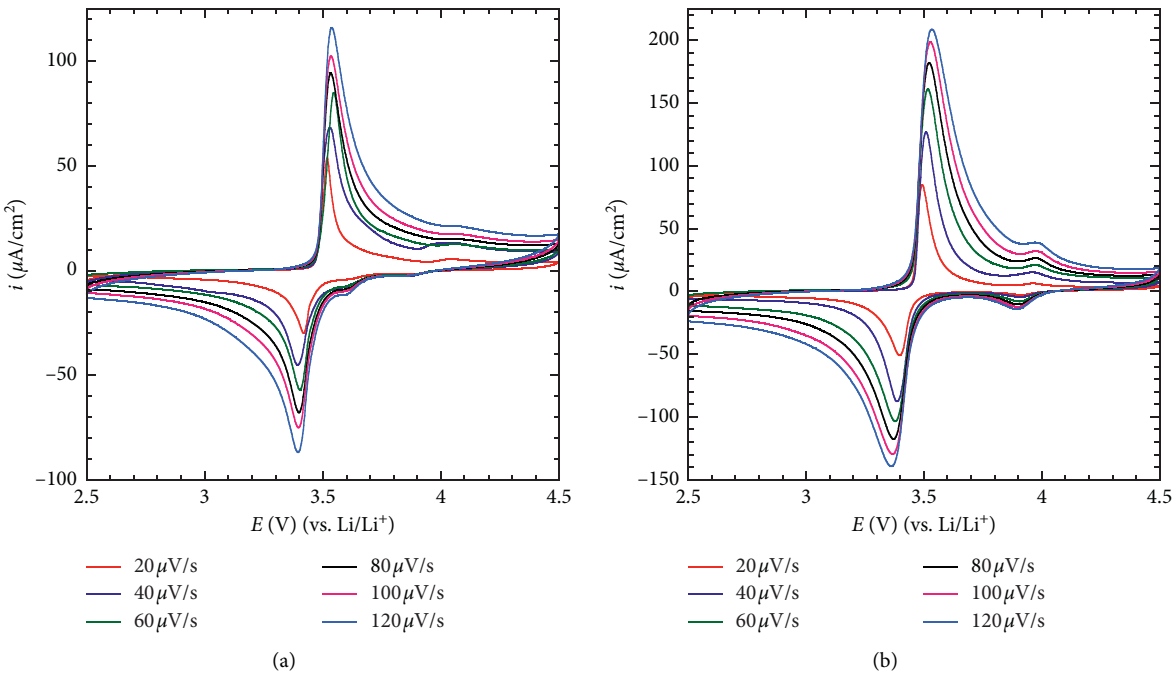

Figure 7: Continued.

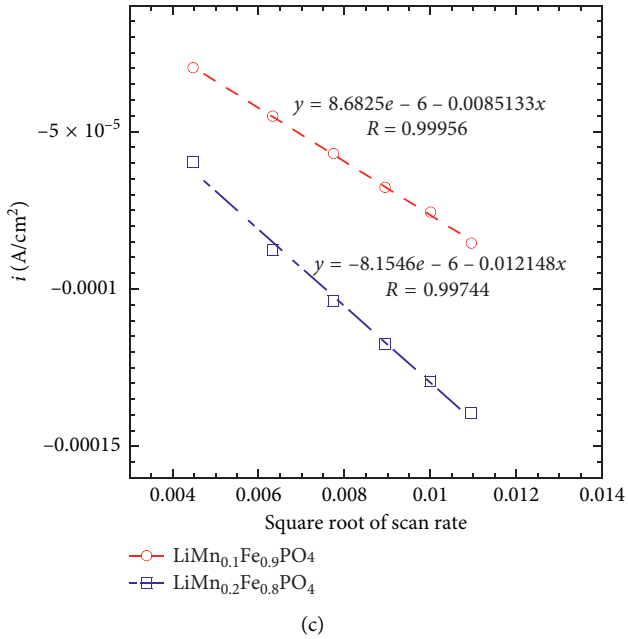

Figure 7: CV curves of $LiMn_{0.1}Fe_{0.9}PO_4$ (a); $LiMn_{0.2}Fe_{0.8}PO_4$ (b), and evolution of i_{pc} in function of root of scan rate (c).

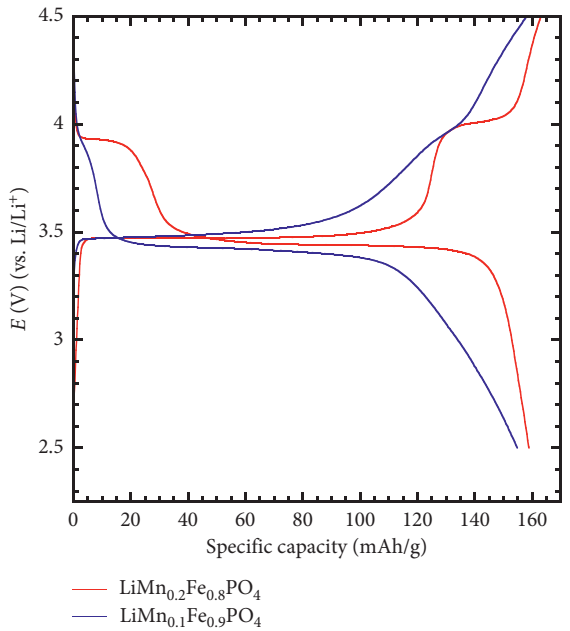

Figure 8: First galvanostatic curves of $LiMn_{0.1}Fe_{0.9}PO_4$and $LiMn_{0.2}Fe_{0.8}PO_4$ at C/10 rate.

Table 3: Lithium diffusion coefficients of $LiMn_{0.1}Fe_{0.9}PO_4$ and $LiMn_{0.2}Fe_{0.8}PO_4$.

	C_M (cm^3/mol)	Slope	D_{Li} (cm^2/s)
$LiMn_{0.1}Fe_{0.9}PO_4$	0.0227	0.0085	2.81×10^{-12}
$LiMn_{0.2}Fe_{0.8}PO_4$	0.0224	0.0121	9.53×10^{-12}

10, C/5, C/2, 1C, 2C, and 5C; an initial capacity of 155 mAh/g is remained at C/10 after 30 cycles. The discharge capacity of $LiMn_{0.2}Fe_{0.8}PO_4$ still seems to be higher, but a slightly fading capacity is also observed. The rate capability performance compares very well with the previous reports on Mn-doped olivines [10, 13].

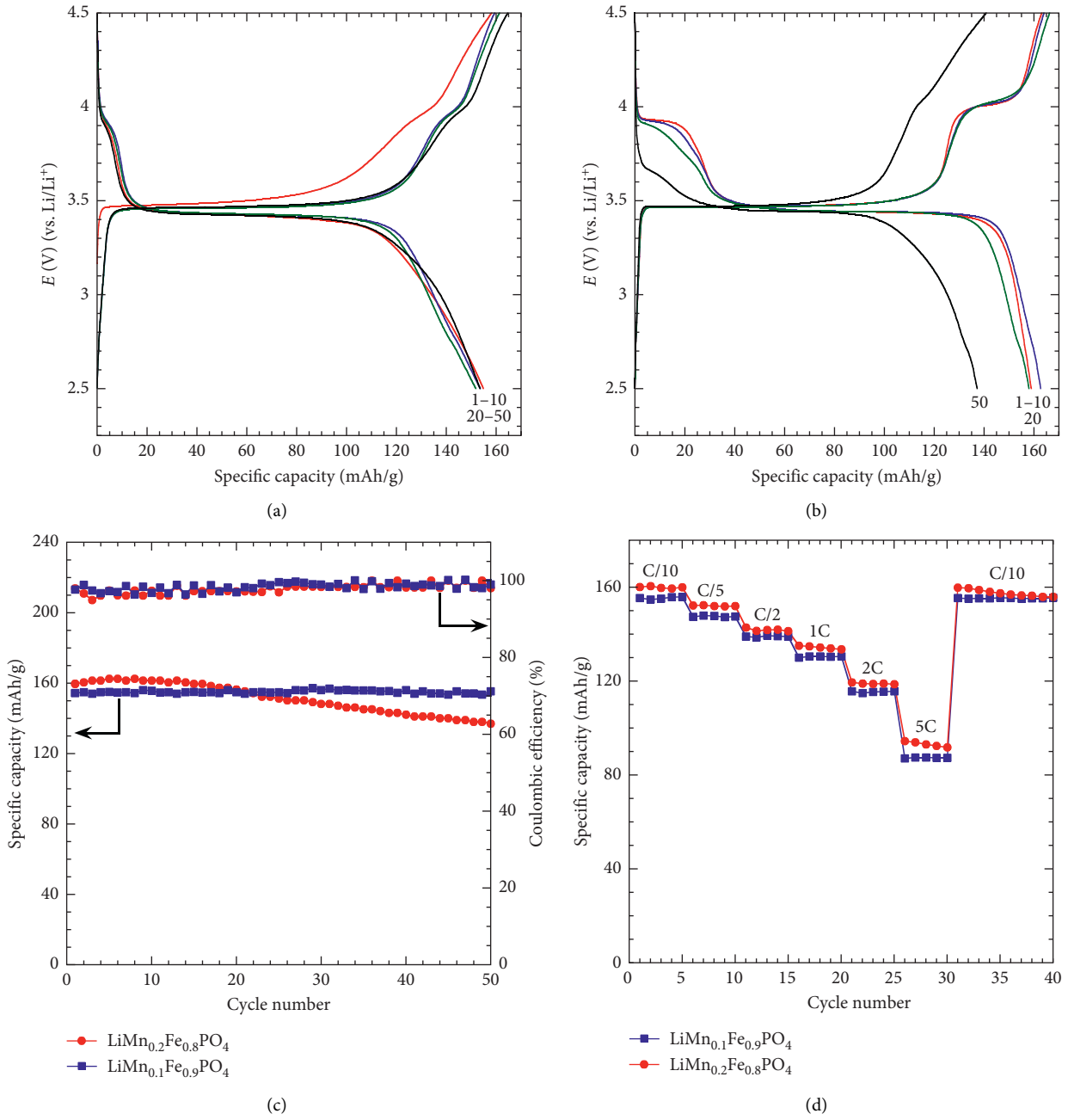

FIGURE 9: Typical galvanostatic curves of $LiMn_{0.1}Fe_{0.9}PO_4$ (a) and $LiMn_{0.2}Fe_{0.8}PO_4$ (b) at C/10 rate; (c) evolution of the specific capacity with cycle number and (d) rate capability performance.

4. Conclusions

In brief, two olivine-type materials $LiMn_{0.1}Fe_{0.9}PO_4$ and $LiMn_{0.2}Fe_{0.8}PO_4$ were successfully synthesized via the hydrothermal route, which present an orthorhombic structure, and their lattice parameters acceded to the preceding reports. Doping Mn can increase the diffusion of Li^+ ions in two orders of magnitude as compared with the original phase $LiFePO_4$. Two Mn-doped olivines showed a stable cycling performance upon 50 cycles as well as rate capability. For the next step, the influence of Mn^{2+} on the activation energy of Li intercalation will be deeply considered.

Data Availability

The data used to support the findings of this study are included within the article.

Conflicts of Interest

The authors declare that they have no conflicts of interest.

Acknowledgments

This work was supported by Vietnam National University Ho Chi Minh (VNUHCM) through grant number C2018-18-11.

References

[1] J.-M. Tarascon and M. Armand, "Issues and challenges facing rechargeable lithium batteries," *Nature*, vol. 414, no. 6861, pp. 359–367, 2001.

[2] B. Scrosati, "Recent advances in lithium ion battery materials," *Electrochimica Acta*, vol. 45, no. 15-16, pp. 2461–2466, 2000.

[3] E. Antolini, "$LiCoO_2$: formation, structure, lithium and oxygen nonstoichiometry, electrochemical behaviour and transport properties," *Solid State Ionics*, vol. 170, no. 3-4, pp. 159–171, 2004.

[4] A. K. Padhi, K. S. Nanjundaswamy, and J. B. Goodenough, "Phospho-olivines as positive-electrode materials for rechargeable lithium batteries," *Journal of the Electrochemical Society*, vol. 144, no. 4, pp. 1188–1194, 1997.

[5] V. Etacheri, R. Marom, R. Elazari, G. Salitra, and D. Aurbach, "Challenges in the development of advanced Li-ion batteries: a review," *Energy & Environmental Science*, vol. 4, no. 9, p. 3243, 2011.

[6] D. Choi and P. N. Kumta, "Surfactant based sol-gel approach to nanostructured $LiFePO_4$ for high rate Li-ion batteries," *Journal of Power Sources*, vol. 163, no. 2, pp. 1064–1069, 2007.

[7] Z. Xu, L. Gao, Y. Liu, and L. Li, "Review—recent developments in the doped $LiFePO_4$ cathode materials for power lithium ion batteries," *Journal of the Electrochemical Society*, vol. 163, no. 13, pp. A2600–A2610, 2016.

[8] T. Nakamura, K. Sakumoto, M. Okamoto et al., "Electrochemical study on Mn^{2+}-substitution in $LiFePO_4$ olivine compound," *Journal of Power Sources*, vol. 174, no. 2, pp. 435–441, 2007.

[9] S. Novikova, S. Yaroslavtsev, V. Rusakov et al., "Behavior of $LiFe_{1y}Mn_yPO_4$/C cathode materials upon electrochemical lithium intercalation/deintercalation," *Journal of Power Sources*, vol. 300, pp. 444–452, 2015.

[10] J. Ding, Z. Su, and H. Tian, "Synthesis of high rate performance $LiFe_{1x}Mn_xPO_4$/C composites for lithium-ion batteries," *Ceramics International*, vol. 42, no. 10, pp. 12435–12440, 2016.

[11] G. Li, H. Azuma, and M. Tohda, "$LiMnPO_4$ as the cathode for lithium batteries," *Electrochemical and Solid-State Letters*, vol. 5, no. 6, p. A135, 2002.

[12] P. Galinetto, M. C. Mozzati, M. S. Grandi et al., "Phase stability and homogeneity in undoped and Mn-doped $LiFePO_4$ under laser heating," *Journal of Raman Spectroscopy*, vol. 41, no. 10, pp. 1276–1282, 2010.

[13] Y. Mi, C. Yang, Z. Zuo et al., "Positive effect of minor manganese doping on the electrochemical performance of $LiFePO_4$/C under extreme conditions," *Electrochimica Acta*, vol. 176, pp. 642–648, 2015.

[14] L. T. N. Huynh, T. T. D. Tran, H. H. A. Nguyen et al., "Carbon-coated $LiFePO_4$-carbon nanotube electrodes for high-rate Li-ion battery," *Journal of Solid State Electrochemistry*, vol. 22, no. 7, pp. 2247–2254, 2018 Jul.

[15] L. T. N. Huynh, H. H. A. Nguyen, T. T. D. Tran et al., "Electrode composite $LiFePO_4$@carbon: structure and electrochemical performances," *Journal of Nanomaterials*, vol. 2019, Article ID 2464920, 10 pages, 2019.

[16] C. Liang, S. Liang, Y. Xia et al., "H_2O-induced self-propagating synthesis of hierarchical porous carbon: a promising lithium storage material with superior rate capability and ultra-long cycling life," vol. 5, no. 34, pp. 18221–18229, 2017.

[17] C. Liang, S. Liang, Y. Xia et al., "Synthesis of hierarchical porous carbon from metal carbonates towards high-performance lithium storage," vol. 20, no. 7, pp. 1484–1490, 2018.

[18] I. Belharouak, C. Johnson, and K. Amine, "Synthesis and electrochemical analysis of vapor-deposited carbon-coated $LiFePO_4$," *Electrochemistry Communications*, vol. 7, no. 10, pp. 983–988, 2005.

[19] D. Y. W. Yu, C. Fietzek, W. Weydanz et al., "Study of $LiFePO_4$ by cyclic voltammetry," *Journal of the Electrochemical Society*, vol. 154, no. 4, pp. A253–A257, 2007.

[20] G. K. P. Dathar, D. Sheppard, K. J. Stevenson, and G. Henkelman, "Calculations of Li-ion diffusion in olivine phosphates," *Chemistry of Materials*, vol. 23, no. 17, pp. 4032–4037, 2011.